PNAS RESEARCH ARTICLE | DEVELOPMENTAL BIOLOGY

microRNA-449a reduces growth hormone-stimulated senescent cell burden through PI3K-mTOR signaling

Sarah Noureddine[a], Jia Nie[b], Augusto Schneider[c], Vinal Menon[d], Zoubeida Fliesen[e], Joseph Dhahbi[e], Berta Victoria[a], Jeremiah Oyer[a], Liza Robles-Carrillo[a], Allancer Divino De Carvalho Nunes[a,d], Sarah Ashiqueali[a], Artur Janusz[a,f], Alicja Copik[a], Paul D. Robbins[d], Nicolas Musi[b,g,h], and Michal M. Masternak[a,i,1]

Edited by Ana Maria Cuervo, Albert Einstein College of Medicine, Bronx, NY; received August 3, 2022; accepted February 5, 2023

Cellular senescence, a hallmark of aging, has been implicated in the pathogenesis of many major age-related disorders, including neurodegeneration, atherosclerosis, and metabolic disease. Therefore, investigating novel methods to reduce or delay the accumulation of senescent cells during aging may attenuate age-related pathologies. microRNA-449a-5p (miR-449a) is a small, noncoding RNA down-regulated with age in normal mice but maintained in long-living growth hormone (GH)-deficient Ames Dwarf (df/df) mice. We found increased fibroadipogenic precursor cells, adipose-derived stem cells, and miR-449a levels in visceral adipose tissue of long-living df/df mice. Gene target analysis and our functional study with miR-449a-5p have revealed its potential as a serotherapeutic. Here, we test the hypothesis that miR-449a reduces cellular senescence by targeting senescence-associated genes induced in response to strong mitogenic signals and other damaging stimuli. We demonstrated that GH downregulates miR-449a expression and accelerates senescence while miR-449a upregulation using mimetics reduces senescence, primarily through targeted reduction of $p16^{Ink4a}$, $p21^{Cip1}$, and the PI3K-mTOR signaling pathway. Our results demonstrate that miR-449a is important in modulating key signaling pathways that control cellular senescence and the progression of age-related pathologies.

senescence | miR-449a | longevity | growth hormone | adipose

Significance

Many neurodegenerative, cardiovascular, and metabolic diseases associated with aging have been linked to the accumulation of senescent cells. Senescence can ultimately lead to tissue dysfunction and inflammation, thereby contributing to disease progression. Novel methods to prevent or attenuate accumulation of senescent cells may help slow progression of age-related pathologies. This study furthers our understanding of the role of miR-449a-5p in regulating key signaling pathways that contribute to senescence and disease progression.

Genetic mutant Ames dwarf (df/df) mice, characterized by growth hormone (GH) deficiency, live 40 to 60% longer than their normal littermates (1, 2). These mice also have improved health span including protection from metabolic syndrome, diabetes, and cancer (2, 3). Although these metabolically heathy df/df mice tend to become obese with age, they maintain high insulin sensitivity (4). Prior studies demonstrated that surgical removal of visceral fat improved insulin sensitivity in normal controls and, however, had the opposite effect in obese df/df mice (4). These findings suggest the endocrine system has varied roles in insulin sensitivity in normal mice versus GH-deficient df/df mice, yet the mechanisms responsible for this altered metabolic function of visceral fat on health and longevity are not well-understood. Since adipose tissue is composed of heterogeneous cell types (5), its cellular composition likely plays a major role in regulating overall health, including insulin sensitivity, glucose metabolism, and inflammation (6).

Progenitor cells, including preadipocytes and adipose-derived stem cells (ADSCs), are important both for tissue health and overall health. Accumulation of changes that compromise tissue function within these cells with time can lead to age-related pathologies (e.g., metabolic diseases neurodegenerative, and cardiovascular pathologies) and give rise to various types of cancers (7). Cellular senescence has a causal role in the progression of these age-related pathologies. Senescence, or rather, the state of proliferative arrest, is triggered by multiple stressors, including DNA damage, oncogenic activation, and exposure to chronic or unbalanced mitogenic signals such as GH, telomere shortening, and chromatin disruption (8).

Although the senescence response can yield beneficial temporal advantages such as tumor suppression or wound repair, the accretion of metabolically active senescent cells (SnCs) can contribute to tissue dysfunction, resulting in pathogenic progression (8). SnCs can alter the tissue microenvironment primarily through the pro-inflammatory senescence-associated secretory phenotype (SASP), which comprises cytokines, chemokines, growth factor metalloproteases, membrane proteins, and extracellular vesicles (9). SASP factors can stimulate various cellular mechanisms in neighboring cells including, but not limited to, cell proliferation, senescence reinforcement, and angiogenesis (9). Despite the apparent transient benefits of the SASP, secretion of the same factors is also linked to the progression of age-related pathologies. The SASP contributes to age-dependent chronic inflammation, a key factor in the pathogenesis of many age-dependent diseases

Author contributions: S.N., A.C., N.M., and M.M.M. designed research; S.N., J.N., A.S., V.M., Z.F., J.O., L.R.-C., A.D.D.C.N., S.A., and M.M.M. performed research; J.D., J.O., L.R.-C., A.D.D.C.N., A.C., N.M., and M.M.M. contributed new reagents/analytic tools; S.N., J.N., A.S., V.M., Z.F., J.D., B.V., J.O., L.R.-C., A.D.D.C.N., A.J., A.C., P.D.R., N.M., and M.M.M. analyzed data; and S.N., J.N., A.S., V.M., Z.F., J.D., B.V., J.O., L.R.-C., A.D.D.C.N., S.A., A.J., A.C., P.D.R., N.M., and M.M.M. wrote the paper.

The authors declare no competing interest.

This article is a PNAS Direct Submission.

[1]To whom correspondence may be addressed. Email: michal.masternak@ucf.edu.

This article contains supporting information online at https://www.pnas.org/lookup/suppl/doi:10.1073/pnas.2213207120/-/DCSupplemental.

Published March 28, 2023.

(7). Hence, reducing SnC burden can decrease age-associated pro-inflammatory signals and pathologies. At the same time, maintaining high populations of healthy progenitor cells can counter the negative impact of senescent cells and, in some cases, even suppress senescence in various tissues.

Some drugs or drug combinations can induce apoptosis specifically in senescent cells; however, these senolytic compounds likely have off-target toxicity (6). As such, identifying a novel method of reducing cellular senescence without severe adverse effects is clinically imperative. Recently, the roles of microRNAs (miRNAs) have been studied due to their ability to target and suppress the translation of messenger RNAs (mRNAs). As a result, miRNAs have been identified as key regulators of many signaling pathways (10, 11) including pathways fundamental for regulating cellular senescence (12). Furthermore, certain miRNAs are associated with increased lifespan and longevity. Studies from our laboratory with long-living GH-deficient df/df mice identified a variety of miRNAs differentially regulated with age (13). One of these miRNAs was microRNA-449a-5p (miR-449a). miR-449a expression decreased significantly with age, yet both long-living GH-deficient mice and older calorie-restricted mice maintained youthful levels of miR-449a in circulation, suggesting its potential role in longevity (13). Additionally, prior studies demonstrated increased senescence is associated with decreased expressions of miR-20a and miR-449a in vitro, with younger phenotypes associated with the latter (12). Thus, there is compelling evidence that miR-449a has therapeutic potential for reducing the progression of age-related pathologies, primarily through regulation of senescence.

Long-living df/df mice also experience reduced senescence onset related to age compared with normal littermates due to GH deficiency (14). One study demonstrated a direct correlation between GH treatment in df/df mice and increased senescence burden, suggesting GH is involved with inducing accelerated senescence in preadipocytes, including adipose-derived stem cells (15). ADSCs typically make up a high proportion of adipose tissue and are essential for tissue repair and regeneration (16). Despite increased intra-abdominal fat accumulation in df/df mice, our previous studies suggest that they have improved metabolic health (4). However, the cellular composition and molecular mechanisms that contribute to the improved metabolic health in df/df mice remain unknown.

Single-cell and single-nuclei sequencing approaches allow in-depth acquisition of genomic and transcriptomic information for identifying differences in cell populations and relationships in a given sample. Such techniques make analyses of molecular mechanisms as well as smaller cell populations and their heterogeneity possible, allowing for characterization of cell populations and the production of cell maps. In this study, single-nuclei sequencing (snRNA-seq) was performed in visceral adipose tissue to compare changes in subpopulations and heterogeneity between df/df mice and phenotypically normal mice. In addition, we evaluated the roles of miR-449a, GH, and adipose-derived stem cells in modulating cellular senescence.

Results

2.1. Df/df Mice Have Elevated Stem Cells, Committed Preadipocytes, and miR-449a in Visceral Adipose Tissue. To capture both mature adipocytes and progenitors, we applied snRNA-sequencing in visceral white adipose tissue (vWAT) freshly isolated from df/df and N/df control male mice. For each condition, we pooled vWAT from two mice prior to snRNA-seq, and four datasets were integrated for further analyses. We identified seven major cell clusters comprising mesothelial cells, spermatozoa, fibroadipogenic precursor cells (FAPs), endothelial cells, mature adipocytes, immune cells, and some unknown cells (Fig. 1). These populations are consistent with published cell populations in mouse epididymal WAT (17), and cell clusters were named accordingly. Preliminary analysis identified that FAPs were increased in df/df mice (Fig. 1 *B* and *C*). Hence, to understand the molecular pathway maps of FAPs, five subpopulations were categorized in our dataset, labeled FAP1, FAP2, FAP3, FAP4, and FAP5 (*SI Appendix*, Fig. S1*A*). In comparison with previously published findings (18), FAP1 represents adipose-precursor cells mainly composed of stem cells, while FAP3 is representative of the committed preadipocytes cluster (*SI Appendix*, Figs. S1 and S2). Both FAP1 and FAP3 populations were elevated in df/df mice, consistent with increased adipose tissue remodeling (*SI Appendix*, Fig. S1 *B* and *C*). This is also consistent with previous findings that df/df mice have healthier adipose tissue and composition (4). Next, we performed differential gene expression analysis for FAPs in normal and df/df mice. Genes highly expressed in df/df mice were enriched for genes encoding proteins involved in insulin signaling and epidermal growth factor receptor (EGFR) signaling, suggesting that these pathways might play an important role in insulin sensitivity and early differentiation of preadipocytes, respectively (*SI Appendix*, Fig. S1*D*).

To validate differences in cell populations within vWAT of df/df mice versus normal littermates, vWAT was isolated, subject to lysis, and analyzed by fluorescence-activated cell sorting (FACS). Using an antibody cocktail containing adipose stem cell markers anti-CD34, anti-Sca-1, anti-lineage, anti-PDGFR-α, and a viability stain (7-AAD), cells were sorted and analyzed based on antibody conjugation (*SI Appendix*, Fig. S4). Compared to phenotypically normal mice, there were considerably elevated numbers of PDGFR-α +, Sca-1 +, and CD-34 + cells (ADSC positive markers) in vWAT extracted from df/df mice (P = 0.0193, Fig. 2*A*). This suggests that df/df mice have a higher percentage of ADSCs. Furthermore, RT-qPCR analysis revealed a significant upregulation of miR-449a in df/df mice compared with N/df mice (P = 0.0191, Fig. 2*B*) and more specifically in ADSCs compared to adipocytes (N P value = 0.0069, df/df P –value = 0.0284, Fig. 2*C*). Similarly, adipose tissue from N/df and df/df mice cultured in media for 72 h demonstrated increased expression of miR-449a in secreted exosomes of the df/df group, suggesting that df/df mice also package and secrete higher amounts of miR-449a than their phenotypically normal littermates (P = 0.01, *SI Appendix*, Fig. S6). Additionally, total RNA-sequencing results identified four miR-449a predicted target genes significantly down-regulated in df/df mice, suggesting that miR-449a is actively suppressing gene targets in vWAT (19) (*SI Appendix*, Table S6). Furthermore, predictive pathway analysis using the DIANA miRPath (v3) micro-T-CDS (v5.0) (20) tool identified Pi3K-AKT signaling as one potential pathway target of miR-449a (*SI Appendix*, Table S1).

2.2. Ames Dwarf Mice Have Reduced Inflammatory Burden and Pi3K-mTOR-Associated Signaling. snRNA-seq results showed that key pathways associated with immune and inflammatory signaling were repressed in the fibroadipogenic precursor cells (cluster comprising stem cells and progenitor cells). These pathways include TGF-β and interleukin-3 signaling pathways (*SI Appendix*, Fig. S1*D*). RNA-sequencing-derived pathway analyses from total vWAT also identified 14 down-regulated and 2 up-regulated immune and inflammatory-related pathways (*SI Appendix*, Table S2). Of the 14 down-regulated pathways, natural killer cell-mediated cytotoxicity, B-cell receptor signaling, chemokine signaling, T-cell receptor signaling, complement and

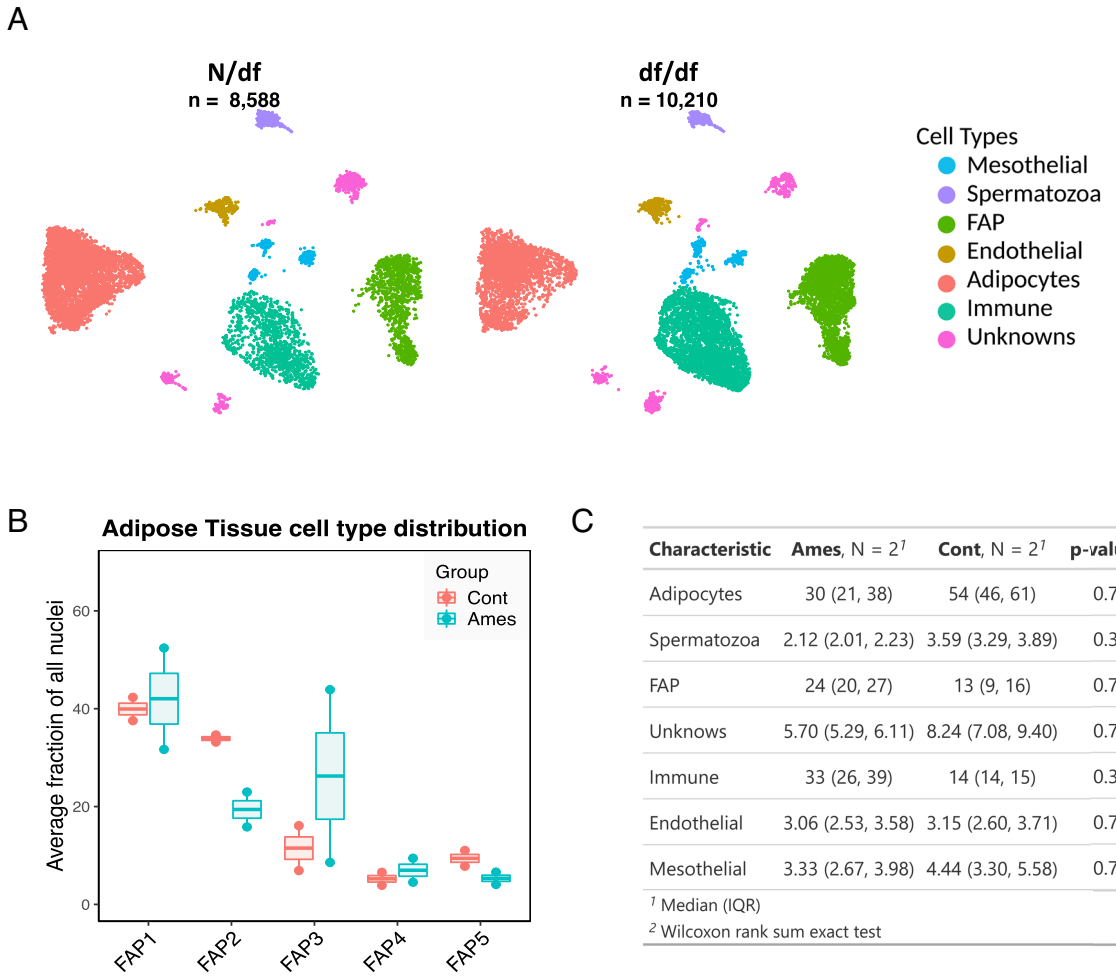

C

Characteristic	Ames, N = 2[1]	Cont, N = 2[1]	p-value[2]
Adipocytes	30 (21, 38)	54 (46, 61)	0.7
Spermatozoa	2.12 (2.01, 2.23)	3.59 (3.29, 3.89)	0.3
FAP	24 (20, 27)	13 (9, 16)	0.7
Unknows	5.70 (5.29, 6.11)	8.24 (7.08, 9.40)	0.7
Immune	33 (26, 39)	14 (14, 15)	0.3
Endothelial	3.06 (2.53, 3.58)	3.15 (2.60, 3.71)	0.7
Mesothelial	3.33 (2.67, 3.98)	4.44 (3.30, 5.58)	0.7

[1] Median (IQR)
[2] Wilcoxon rank sum exact test

Fig. 1. Single-nuclei sequencing reveals higher percentage of fibroadipogenic precursor cells in visceral adipose tissue of df/df mice. (*A*) Different cell populations within visceral adipose tissue distinguished by color. Embedding is based on the 1,000 most variable genes and the first 15 harmonized principle components. Clustering was performed on the UMAP embedding. (*B*) Fraction (relative to the total number of nuclei) of each cell type in within visceral adipose tissue of control and df/df mice. (*C*) Quantification of cell populations shown in *A* as percentages of total population.

coagulation cascades, Toll-like receptor signaling, JAK-STAT signaling, proteasome, and regulation of actin cytoskeleton were significantly down-regulated in df/df mice. This is consistent with the reduced inflammatory burden in adipose tissue of df/df mice. Additionally, pathways influenced by PI3K-AKT signaling cascades, such as oxidative phosphorylation and JAK-STAT signaling pathways, were significantly down-regulated in total vWAT (*SI Appendix*, Table S3) (21). The VEGF, p53, ErbB, and MAPK signaling pathways were also down-regulated. In contrast, insulin signaling was increased in FAPs, suggesting its importance in vWAT remodeling (*SI Appendix*, Fig. S1*D*).

2.3. Senescence-Associated Genes Are Differentially Expressed in Long-Living Ames Dwarf Mice. To determine if long-living df/df mice are less susceptible to senescent burden (14), RNA was extracted from vWAT of df/df mice and N/df mice and outsourced for RNA-sequencing. We identified 10 differentially expressed genes in df/df mice associated with the senescence phenotype (*SI Appendix*, Table S4). Of these genes, *Ksr2, Hla-g, Cdkn2a* ($p16^{Ink4a}$), *Fos, Galectin-3*, and *Pai-1* are linked with inducing or promoting senescence when up-regulated (22). These genes were significantly down-regulated in df/df mice compared to N/df littermates. Further, genes typically associated with anti-senescence activity (including *Pdzd2*, *Arg-Bp2*, *Vegf-a*, *Notch3*, and *Bcl6b*) were significantly up-regulated in df/df mice. Analysis of senescence scores across cell types in snRNA-Seq of df/df vWAT compared to phenotypically normal mice also demonstrated reduced senescence onset specifically in adipocytes, endothelial, immune, spermatozoa, and unidentified cell types (*SI Appendix*, Fig. S3*A*), while FAP subtypes did not reveal significant deviations in senescence (*SI Appendix*, Fig. S3*B*). These results suggest that GH-deficient df/df mice are less susceptible to both SnC burden and inflammation.

2.4. miR-449a Regulates the Senescence Pathway under Senescence-Inducing Conditions. Human umbilical vein endothelial cells (HUVECs) were cultured under normal conditions with RNA isolated at different passages (3, 5, 7, and 13), and levels of miR-449a decreased as HUVECs were sequentially passaged. At passage 13, there was no detectable miR-449a expression (*SI Appendix*, Fig. S8*A*). Furthermore, senescence-associated β-galactosidase staining revealed an increase in SnCs with increasing passage number, suggesting that miR-449a and senescence are inversely associated (*SI Appendix*, Fig. S8*B*). To determine whether miR-449a regulates cellular senescence, $p21^{Cip1}$ and *p53* mRNA transcript levels were quantified in conjunction with senescence-associated β-galactosidase staining in HUVECs transfected with either a miR-449a mimic or miR-449a inhibitor. Post-transfection miR-449a levels were compared to endogenous miR-449a levels to validate transfections ($P < 0.0001$; *SI Appendix*,

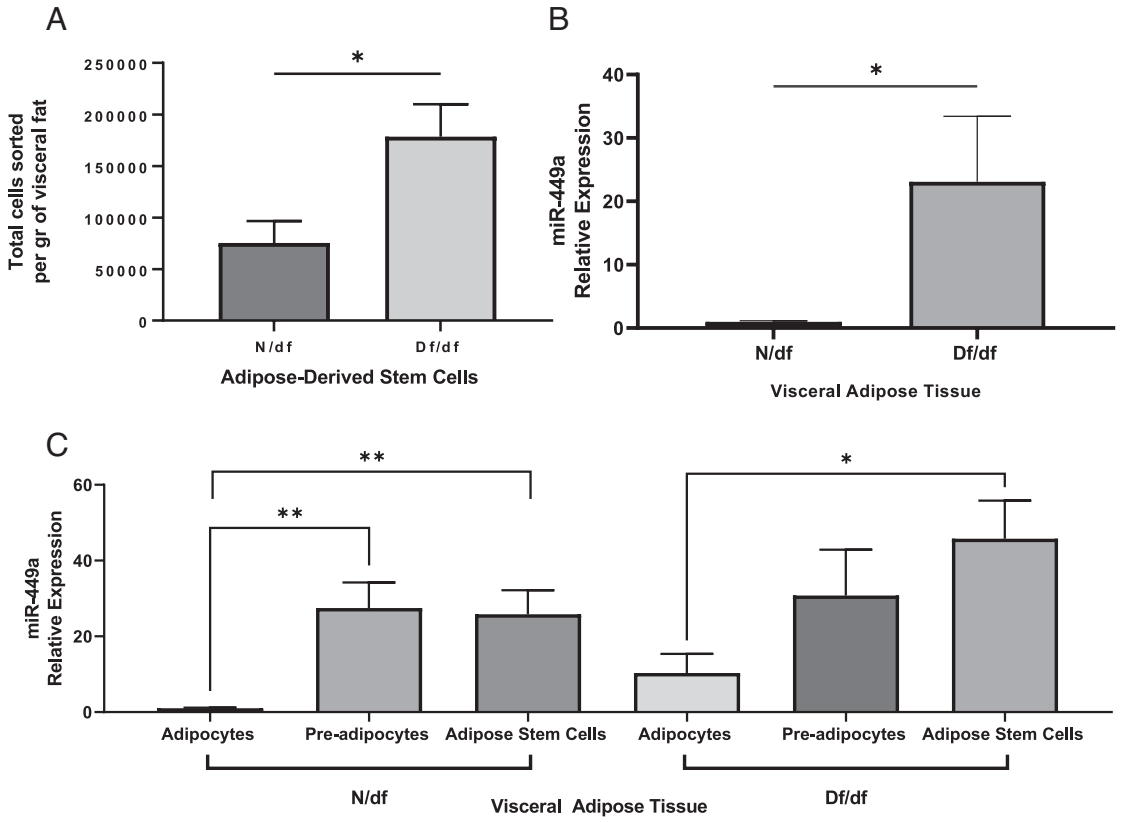

Fig. 2. Fluorescence-activated cell sorting reveals higher number of adipose-derived stem cells and qRT-PCR demonstrates elevated miR-449a in total adipose tissue, adipose-derived stem cells, and preadipocytes isolated from df/df mice versus controls. (*A*) Total cells sorted per gram of visceral fat gated for live, lineage (−), PDGFRα (+), Sca-1 (+), and CD34 (+) populations. (*B*) Relative expression of miR-449a in visceral adipose tissue determined by quantitative RT-PCR. (*C*) Relative expression of miR-449a in sorted cells in visceral adipose tissue of N/df and df/df mice. Relative expression was calculated using the $2^{-\Delta\Delta CT}$ method. Statistical analyses used independent *t* test (two groups) or one-way analysis of variance with multiple comparisons (Tukey's test). Values depicted as mean ±SEM. **P* value < 0.05, ***P* value < 0.01, ****P* value < 0.001.

Fig. S7 *A* and *B*). Inhibition of miR-449a was associated with increased expression of $p21^{Cip1}$ compared to controls, whereas *p53* levels were significantly increased in the miR-449a inhibitor group compared with mimic transfected cells (*SI Appendix*, Fig. S8 *E* and *F*) ($P = 0.0263$). Percentages of β-galactosidase-positive cells in the miR-449a inhibitor group significantly increased, suggesting that inhibiting miR-449a promotes a marked increase in senescent cells ($P = 0.0036$; Fig. 3*A*). These results suggest that the inhibition of miR-449a contributes directly to the onset of senescence.

In GH-treated cells, miR-449a levels were significantly down-regulated, suggesting that GH has a regulatory role in modulating miR-449a levels ($P = 0.0013$; *SI Appendix*, Fig. S8*C*). To evaluate this further, HUVECs were subjected to GH and transfected with miR-449a mimic and inhibitor during exposure. Inhibition of miR-449a activity increased both $p16^{Ink4a}$ and $p21^{Cip1}$ levels in vitro ($P = 0.0048$ and <0.0001, respectively) (Fig. 4 *A* and *B*). These findings are further validated by the increased percentage of SA-βgal+ cells in both the inhibitor and control groups ($P = 0.0013$ and 0.0002, respectively; Fig. 3*B*). Further, overexpression of miR-449a under GH exposure significantly reduced the senescent profile of cells in the control and inhibitor groups ($P = 0.0343$ and 0.0038, respectively; Fig. 3*B*). Hence, miR-449a suppressed the onset of senescence in response to GH stimulation.

This reduction in senescence onset may be modulated through the PI3K-AKT signaling pathway (*SI Appendix*, Table S1). Previous studies have linked increased Pi3K and mTOR activity to reduced longevity (23). Consistent with those results, we found that the PI3K-AKT signaling pathway is regulated by miR-449a overexpression (Fig. 4 *D* and *E*), suggesting that senescence may be hindered through the modulation of *Pi3ka* and *mTOR*. In addition to the observed reduction in *Pi3ka* and *mTOR*, *Foxo1* expression was also reduced; *Foxo1* is typically up-regulated when PI3K-AKT signaling is down-regulated (23). Increased FOXO1 activity is associated with promoting apoptosis (24); hence, miR-449a could suppress senescence without promoting apoptosis. To confirm this, we carried out flow cytometry analysis of apoptosis and cell death in miR-449a mimic and inhibitor-transfected HUVECs. As surmised, miR-449a upregulation did not promote apoptosis (*SI Appendix*, Fig. S11).

2.5. miR-449a Transfected ADSCs Promote Senescence Rescue after Induction In Vitro. To assess the therapeutic potential of miR-449a, HUVECs were cultured under GH treatment (5 nM) for 5 d and then cocultured with miR-449a transfected (20 nM) and nontransfected (control) ADSCs for an additional 5 d. Posttransfection miR-449a levels were compared to endogenous miR-449a levels to validate transfections ($P = 0.0004$; *SI Appendix*, Fig. S7*C*). In HUVECs cultured with transfected ADSCs, miR-449a levels were significantly increased, suggesting that miR-449a is being packaged and distributed by these cells ($P = 0.0021$; Fig. 5*A*). To verify this notion, exosomes isolated from the media of control and transfected ADSCs were subject to RNA extraction, cDNA prep, and quantitative RT-PCR. miR-449a levels were significantly increased in the exosomes collected from transfected ADSCs ($P = 0.0392$; *SI Appendix*, Fig. S10*A*). However, to ensure that HUVECs were taking in the miR-449a packaged and released by the stem cells, we fluorescently labeled and treated HUVECs

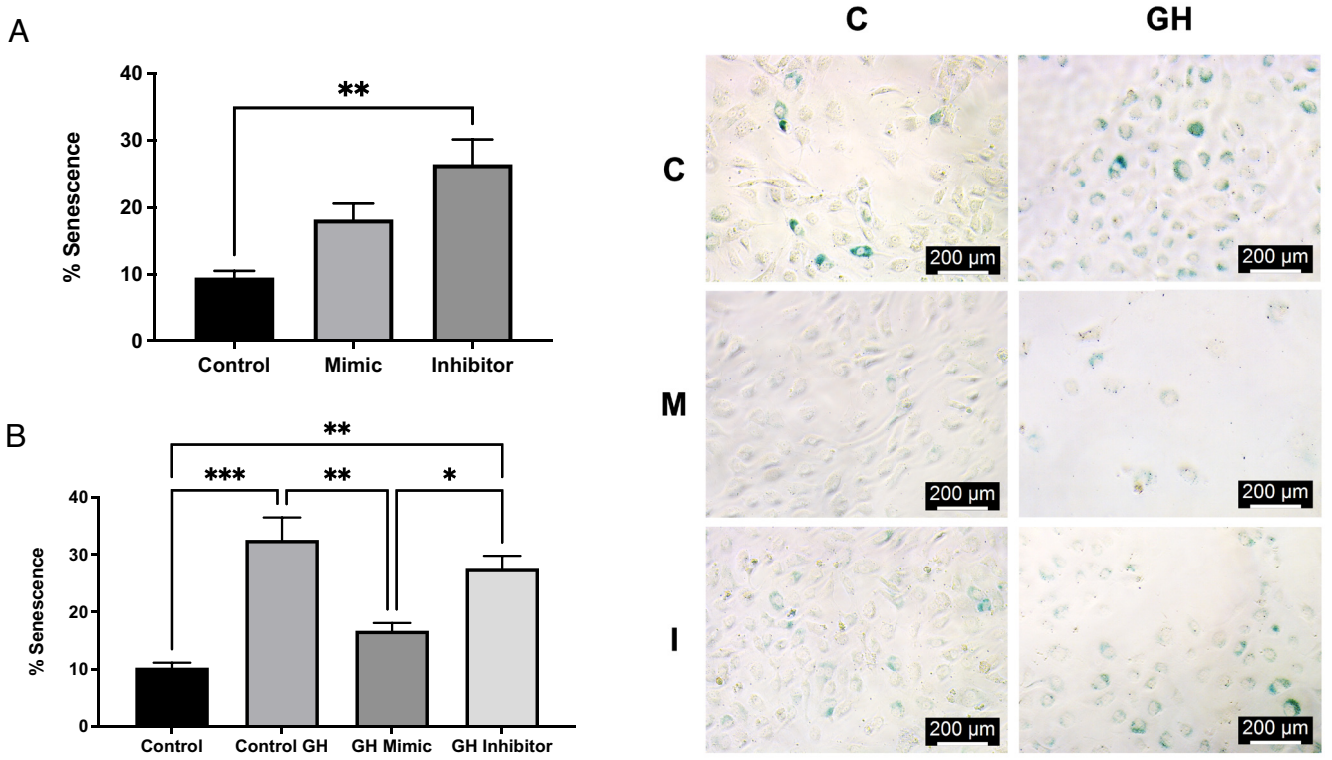

Fig. 3. Senescence-associated β-galactosidase activity is suppressed in miR-449a mimic-HUVECs. (*A*) Percentage of senescence-positive cells in control, miR-449a mimic-transfected, and miR-449a inhibitor-transfected HUVECs (n = 4 per group). (*B*) Percentage of senescence-positive (blue stained) cells in control (C), mimic-transfected (M), and inhibitor-transfected (I) HUVECs treated with 5 nM growth hormone (GH) for 10 d versus untreated controls (n = 4 per group). Blue color is produced in the presence of X-gal and β-galactosidase, wherein the enzyme β-galactosidase (highly expressed in senescent cells) cleaves X-gal to produce the observed blue color. Statistical analyses used one-way analysis of variance with multiple comparisons (Tukey's test). Values are mean ± SEM. **P* value < 0.05, ***P* value < 0.01, ****P* value < 0.001.

with isolated exosomes from transfected and control ADSCs. Our findings demonstrated localized uptake of the labeled exosomes (represented by green fluorescence) followed by increased miR-449a in treated HUVECs (*SI Appendix*, Fig. S10 *B–E*) ($P < 0.0001$). Further, a reduction in $p21^{Cip1}$ ($P = 0.0325$), *Ccnd1* ($P = 0.0443$), and *Foxo1* ($P = 0.0451$) levels was also observed, with an apparent reduction in PI3K/mTOR signaling, *Tnf-α,* and *Interleukin-1a (Il-1a)* (Fig. 5 *B–I*) in cocultured HUVECs. These findings indicate miR-449a has a robust regulatory role in the expression of senescence-associated genes.

Discussion

Visceral adipose tissue is essential for adaptations in response to metabolic changes throughout the body. Although snRNA-seq methods have greatly advanced current approaches to understanding the cellular and molecular compositions of tissue, characterization of visceral adipose tissue has not been fully explored. Previously, white adipose tissue was sequenced for identification of cell subtypes in different mouse models. Seven distinct clusters based on gene expression and pathway analysis were identified in epididymal white adipose tissue (eWAT) of DLK1-RFP male mice; five were designated as adipocytes, FAPs, immune cells, endothelial cells, and mesothelial cells. FAPs constitute stem cells, preadipocytes, and fibroblasts. Within these, there are four subpopulations (FAP1, FAP2, FAP3, and FAP4). According to differential gene expression and pathway analysis, FAP3 primarily consists of preadipocytes. Based on these classifications, Sarvari et al. compared their clusters to previously identified FAP subpopulations. FAP3 closely resembled ICAM1+ clusters (25), adipose stem cell 1 (ASC1) clusters (26), adipocyte progenitor and committed preadipocyte clusters (18), and P2 progenitor clusters (27). Although previously identified subpopulations were clustered differently, the FAPs identified were highly similar (17). In the current study, we clustered the results of single-cell sequencing analyses of vWAT of df/df and N/df (control) mice using a similar approach. We observed that df/df mice have more stem cells/progenitor cells and committed preadipocytes than N/df mice.

Our findings also suggest that GH-deficient long-living df/df mice exhibit reduced senescence in adipose tissue, likely from the absence of GH. Prior studies have determined that df/df mice have healthier adipose tissue that contributes to their increased lifespan while others have determined that GH-deficient mouse models demonstrate reduced senescence burden in their adipose tissue (28, 29). These findings are consistent with our total RNA and snRNA-sequencing results, which revealed that GH-deficient df/df mice have altered adipose composition and fewer markers of senescence, senescence-associated secretory phenotype (SASP), and inflammation. Additionally, our findings support the hypothesis that adipose remodeling is increased in df/df mice, exhibited by their greater transition between preadipocytes/progenitor cells to adipocytes. This increase in adipocyte production may contribute to their altered adipose composition and associated health benefits. These results are also consistent with a previous report demonstrating that the absence of GH action resulted in delayed age-related senescent cell (SnC) accumulation and down-regulated expression of prominent senescent markers ($p16^{Ink4a}$ and $p21^{Cip1}$) in adipose tissue (15).

Various studies have attributed the reduced senescent burden in df/df mice to altered adipose tissue function (14). Our results suggest a potential link between reduced expression of pro-senescence genes and inflammatory and PI3K-AKT and

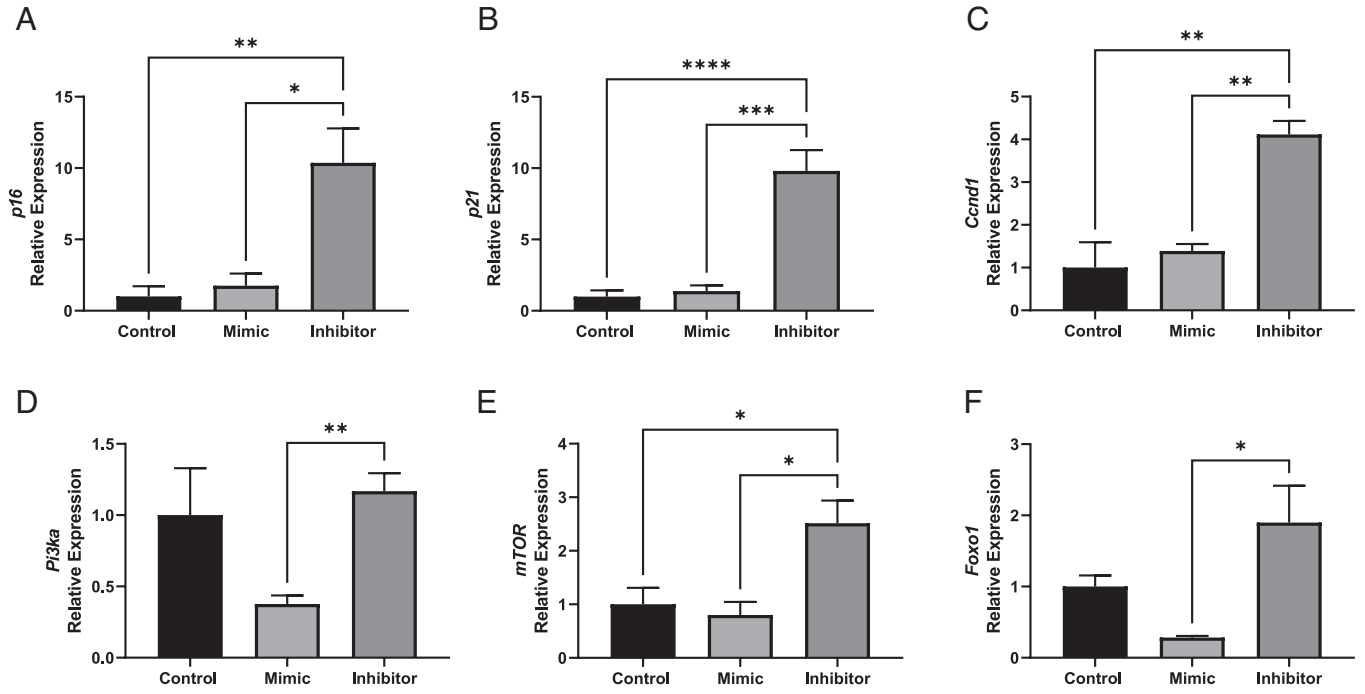

Fig. 4. miR-449a regulates pro-senescence genes and modulates the Pi3K-mTOR signaling pathway with growth hormone (GH) treatment. (*A* and *B*) Relative expression of senescence markers *p21* and *p16* quantified with RT-PCR in GH-treated and transfected HUVECs. (*C*) Relative expression of miR-449a target *Ccnd1* in control, mimic-transfected, and inhibitor-transfected cells. (*D* and *E*) Relative expression of *Pi3ka* and *mTOR* in control, mimic-transfected, and inhibitor-transfected cells. (*F*) Relative expression of *Foxo1* with GH treatment. Relative expression (n = 4 per group) was quantified through RT-PCR and calculated using the $2^{-\Delta\Delta CT}$ method. Statistical analyses used independent *t* test (two groups) or one-way analysis of covariance with multiple comparisons (Tukey's test). Values are mean ± SEM. **P* value < 0.05, ***P* value < 0.01, ****P* value < 0.001, *****P* value < 0.0001.

mTOR signaling pathways. Previous studies have associated increased mTOR activation with replicative cellular senescence. Rapamycin, an mTOR inhibitor, blocks mTORC1 activity and has been used to treat diseases related to aging such as cancer, diabetes, and obesity (30); it also promotes increased longevity in animal models of aging (31). GH signaling activates mTOR through PI3K-AKT signaling (32), which then activates MAPK signaling pathways. Reduced AKT activity is associated with reduced cellular senescence and improved longevity (33). Thus, the lower senescent burden we observed in GH-deficient df/df mice may be due to increased regulation of the PI3K-AKT signaling pathway in vWAT. Our analysis of visceral adipose content in df/df mice revealed elevated levels of ADSCs, a cell type that confers resistance to oxidative stress-induced senescence and increases angiogenesis (34).

Long-living df/df mice express higher levels of miR-449a in both total vWAT and in ADSCs, while also displaying elevated miR-449a in exosomes released by vWAT. These findings are further validated by our previous analysis of circulating miRNAs in df/df and N/df mice, wherein miR-449a expression decreased with normal aging but was consistent in df/df mice with age (13). Predictive pathway analysis also demonstrates a potential for miR-449a to modulate the Pi3K-AKT-mTOR pathway. Based on the literature, miR-449a regulates the differentiation of mesenchymal stem cells (35) and has previously been implicated in promoting senescence in cancer or tumor cell lines (36). However, based on the presented findings, miR-449a is associated with the opposite phenotype in noncancer cell lines, reducing senescence in HUVECs. In addition, treatment with GH decreases miR-449a levels in HUVECs while increasing the percentage of SnCs.

When we quantified the expression of miR-449a in sequentially passaged HUVECs, miR-449a expression decreased with higher passage numbers. Conversely, the percentage of SnCs increased with higher passage numbers. Previously, in senescence-accelerated mouse prone 8 (SAMP8) mice, miR-449a levels were significantly reduced with age, but in senescence-accelerated mouse resistance 1 (SAMR1) mice, miR-449a levels remained unchanged (37). These findings support the associations between age and miR-449a and senescence and miR-449a. In HUVECs treated with GH for an extended period, we found that senescence increased in the GH-treated group as well as in the miR-449a inhibitor-transfected group. However, HUVECs transfected with miR-449a mimic were rescued from the senescent burden with miR-449a upregulation reducing senescence comparable to untreated controls, once again reinforcing the hypothesis that miR-449a expression is necessary for regulating senescence. Expression of $p16^{Irk4a}$ and $p21^{Cip1}$ was significantly increased in the miR-449a inhibitor-transfected group, further confirming the senescent profile.

As a control for the function of the miR-449a inhibitor, *Cyclin D1*, a target of miR-449a, was quantified through RT-qPCR and was found to be increased in the inhibitor group (19). Although the control group did not exhibit increased $p16^{Irk4a}$ and $p21^{Cip1}$ expression at the mRNA level, β-galactosidase activity was significantly higher in both the control and inhibitor groups, suggesting that senescence is indeed induced by GH. In addition, miR-449a upregulation appears to regulate the expression of *Pi3ka,* suggesting the PI3K-AKT pathway is modulated under GH treatment. This is complemented by a marked increase in *mTOR* expression in the inhibitor GH-treated group, suggesting miR-449a inhibition results in altered expression of *mTOR*. Similarly, predictive pathway analysis suggests that miR-449a interferes with the Pi3K-AKT signaling pathway, a notion supported by the presented data. Although *Foxo1* expression was also modulated, this may be attributed to a negative regulation of apoptosis otherwise induced by increased FOXO1 expression (24). Hence, miR-449a may inhibit senescence by regulating *p16/p21* and *Pi3k-mTOR* expression while also modulating apoptosis to ensure cell survival through suppression of *Foxo1*. This notion was validated by our

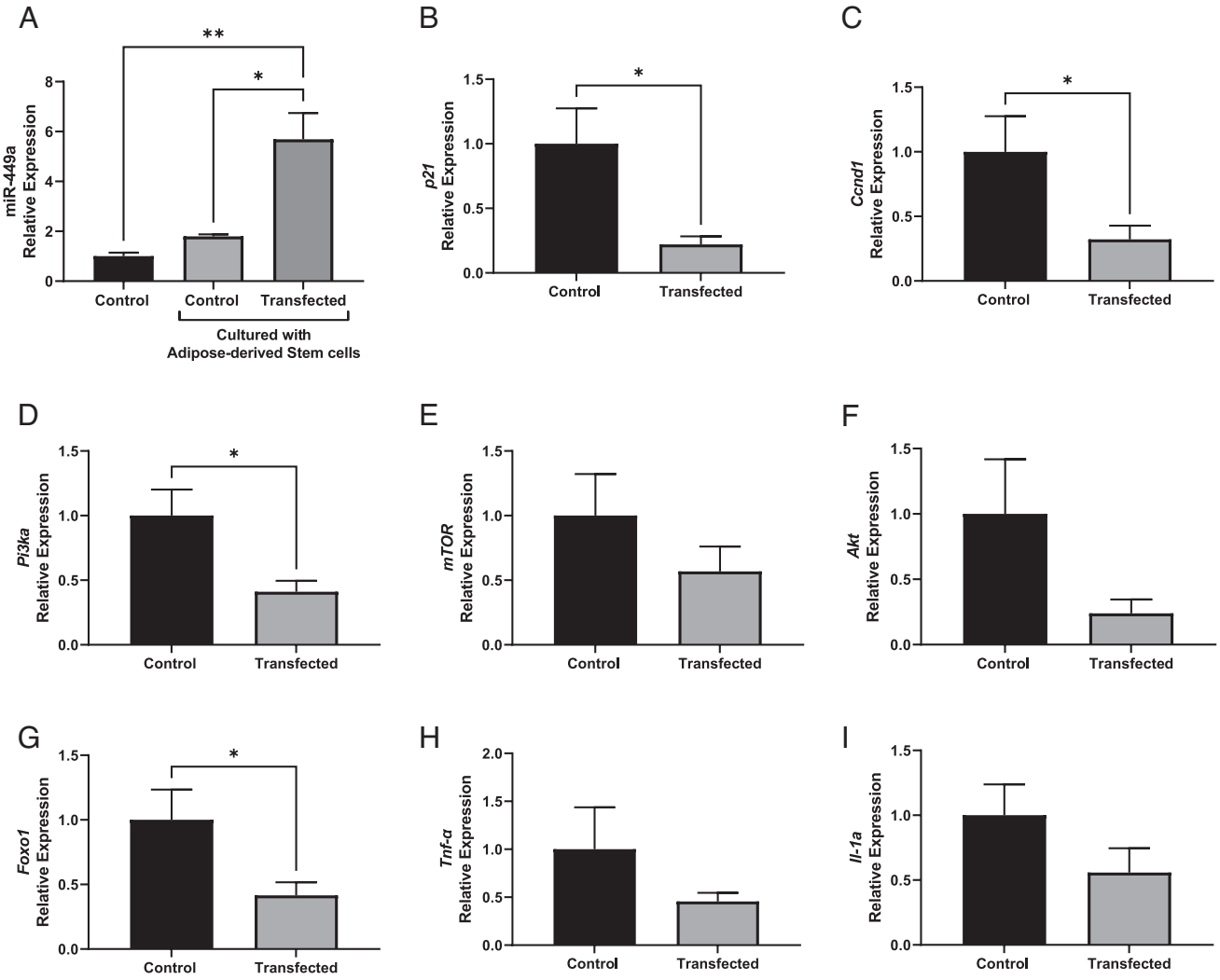

Fig. 5. miR-449a uptake in cocultured HUVECs secreted by adipose-derived stem cells (ADSCs) regulates pro-senescence genes and modulates Pi3K-mTOR signaling with growth hormone (GH) treatment. (*A*) Relative expression of miR-449a in control HUVECs, HUVECs cocultured with control ADSCs, and HUVECs cocultured with transfected ADSCs. (*B–I*), Relative expression of *p21, Cyclin D1 (Ccnd1), Pi3ka, mTOR, Foxo1, Tnf-α,* and *Interleukin-1α (Il-1α)* in GH-treated HUVECs cocultured with nontransfected ADSCs (control) and transfected ADSCs. Relative expression (n = 4 per group) was quantified through RT-PCR and calculated using the $2^{-\Delta\Delta CT}$ method. Statistical analyses used independent *t* test (two groups) or one-way analysis of variance with multiple comparisons (Tukey's test). Values are mean ± SEM. **P* value < 0.05, ***P* value < 0.01.

flow cytometry analyses, wherein the percentage of live cell populations was significantly higher in mimic-transfected HUVECs compared to controls. These findings may elucidate how the PI3K-AKT-mTOR signaling in df/df mice is regulated to favor increased lifespan through reduced senescence burden.

Since df/df mice express higher levels of miR-449a and have an increased proportion of adipose-derived MSCs, we aimed to identify the effect of transfecting human ADSCs with miR-449a in coculture with GH-treated HUVECs. Under senescence-inducing conditions promoted by GH exposure, miR-449a levels were increased in HUVECs cocultured with ADSCs transfected with miR-449a while $p21^{Cip1}$ and SASP factors *Tnf-α* and *interleukin-1a* levels were down-regulated, suggesting that miR-449a is modulating senescence. In addition, *Pi3ka* and *mTOR* expression levels were also down-regulated by miR-449a, confirming our previous experiments.

ADSCs have been beneficial in reducing age-related pathologies primarily due to their ability to differentiate into different lineages and have shown therapeutic promise when transfected with miR-449 (38). Further, ADSCs have improved healing and pain in clinical studies (39) and are linked to the release of paracrine factors associated with promoting regeneration (40). Consistent with these earlier reports, preliminary findings from our lab revealed high levels of miR-449a in exosomes isolated from transfected ADSCs. Thus, it appears that stem cells can also rescue senescence in GH-treated HUVECs through miR-449a secretion. We also found that levels of $p21^{Cip1}$, *Tnf-α, interleukin-1a, Foxo1, Pi3ka*, and *mTOR* expression were down-regulated in these conditions, contributing to overall reduced senescence burden and cell survival. These findings suggest a potential therapeutic role of miR-449a in reducing senescence burden through adipose-derived MSCs. Our results also suggest that exosomes secreted by ADSCs effectively deliver packaged miR-449a to neighboring cells to potentially reduce senescence, a notion validated by our study involving fluorescently labeled exosomes isolated from transfected and control stem cells that were established to be taken up by recipient HUVECs through fluorescence microscopy.

Hence, our findings suggest that lipid-tagged miR-449a or exosomes isolated from ADSCs containing miR-449a could reduce senescence/SASP and improve metabolic health. Overall, our findings support the notion that miR-449a could be therapeutically

implemented to reduce senescence burden and delay the onset of age-related pathologies associated with cellular senescence.

Materials and Methods

4.1. Mice and Tissue Collection. Phenotypically normal heterozygous females (N/df) were mated with homozygous Ames dwarf (df/df) males to produce offspring with both normal (N/df) and df/df phenotypes. Mice were bred under controlled temperatures and light cycles and placed on a nutritionally balanced diet (Rodent Laboratory Chow 5001) provided ad libitum. For RNA sequencing, male offspring (8 to 12 mo of age) were divided into normal (N/df, n = 4) and dwarf (df/df, n = 5) groups. Mice were anesthetized with 2.5% isoflurane and sacrificed following overnight fasting for serum and tissue collection. Harvested tissue was immediately snap-frozen on dry ice and stored at −80°C.

To perform fluorescence-associated cell sorting (FACS), both male N/df (n = 7) and df/df (n = 7) mice were used. Mice were anesthetized with isoflurane and sacrificed as described previously prior to tissue collection. Skin was disinfected with 70% ethanol prior to adipose depot removal. vWAT obtained from N/df and df/df mice was transferred to 50 mL conical tubes containing 10 mL of ice-cold buffer containing HBSS, 2% FBS, and HEPES (Gibco™, Waltham, MA). All collected vWAT was weighed to ensure that at least 1 g of fat was included and kept on ice. Collected adipose tissue was separated for culturing and for tissue lysis and digestion. Minced tissue (1 to 2 mm in size) was digested using 0.8 mg/mL Gibco™ collagenase (Type II) diluted in 5 mL of wash buffer and then incubated in a shaking water bath (120 to 140 rpm) for 60 min at 37 °C. Following incubation, samples were centrifuged at 300 × g for 10 min at 4 °C to separate adipocytes (white layer on top) from stromal vascular cells (preadipocyte precursors; red/white pellet at the bottom). Separated cells were then prepared for FACS (refer to supplemental methods section 1.1). Separately, cultured adipose tissue was lightly minced and grown in six-well culture plates (Corning, Glendale, AZ) with MEM Alpha (1X) manufactured by Gibco™ supplemented with 10% exosome-depleted FBS (System Biosciences). Media from cultured adipose tissue was collected following 72 h for exosome isolation using the Total Exosome RNA and Protein Isolation Kit For isolation of RNA and protein from exosomes (ThermoFisher Scientific). cDNA prep and RT-qPCR were performed as described in *SI Appendix, Supplemental Methods Section 1.2*.

4.2. 10x Genomics and RNA Sequencing (Single-Nuclei Sequencing). Isolation of nuclei from adipose tissue was performed as described in supplemental methods section 1.3. The GemCode Single-Cell Instrument (10x Genomics) and Single Cell 3 Library & Gel Bead Kit v3.1 Kit (10× Genomics) were utilized for single-cell analyses and library preparation. About ~17,400 nuclei were added to each channel with a targeted cell recovery estimate of 10,000 cells. After generating nanoliter-scale Gel bead-in-EMulsions (GEMs), GEMs were reverse-transcribed in a T100 Thermal cycler (Bio-Rad) programmed at 53 °C for 45 min, 85 °C for 5 min, and held at 4 °C. All subsequent steps to generate single-cell libraries were performed according to the manufacturer's protocols. Libraries were sequenced with an Illumina NovaSeq 6000 System (North Texas Genome Center, University of Texas at Arlington), with approximately 80,000 raw reads per nucleus. The libraries were sequenced with the following sequencing parameters: 26 bp read 1 to 8 bp index 1 (i7)–88 bp read 2.

4.3. RNA Sequencing of Total vWAT. Visceral fat obtained from N/df (n = 4) and df/df (n = 5) male mice were cut and weighed to obtain approximately 30 mg of tissue for RNA extraction. Samples were homogenized in a bullet blender using 500 µL of QIAzol Lysis Reagent and 0.5 mm zirconium oxide beads for 3 min. An additional 400 µL of QIAzol Lysis Reagent was added to each sample following tissue lysis. After complete tissue homogenization was achieved, the manufacturer's protocol was used in accordance with the RNeasy mini kit (QIAGEN; Hilden, Germany). The purified total RNA was then eluted using 30 µL of RNase-free water, and nucleic acid quantification was performed using the Epoch Gen5 Plate Reader. One µg of total RNA isolated from each tissue sample was used to construct sequencing libraries with the NEBNext Ultra Directional RNA Library Prep Kit for Illumina (San Diego, CA), following the manufacturer's protocol. Libraries were submitted for 100-bp paired-end sequencing by Illumina HiSEQ 2000 at the Genomics Core in the University of California Riverside (UCR) Institute of Integrated Genome Biology.

4.4. Cell Culture. Human umbilical vein endothelial cells (HUVECs) were included in this study for their ease of transfecting and lack of differentiative capacity when treated with GH. HUVECs were cultured using Endothelial Cell Growth Media plus supplement [without vascular endothelial growth factor (VEGF)] (R&D Systems). Adipose-derived stem cells (ADSCs) were cultured using MEM Alpha (1X) manufactured by Gibco™ supplemented with 16% FBS and 1% L-glutamine. Coculture media was prepared by combining Basal Cell Culture Liquid Media DMEM/F12 (Corning, Corning, NY) (50:50 mix) with endothelial cell growth supplement and 10% FBS. All combined media and supplement were vacuum-filtered using a Corning Disposable Vacuum Filter (0.2-µm pore size)/Storage systems prior to usage. Cells were grown at 37 °C in a 5% CO_2 incubator. Media was changed every 48 h and when confluent, cells were passaged using 0.05% Trypsin-EDTA (1X), phenol red (Gibco™). To quantify cell density, a 1:1 dilution of cell mixture to Trypan Blue Solution, 0.4% (Gibco™) was prepared and transferred to a hemocytometer/counting chamber for automated counting using the Corning® Cell Counter. Based on cell density, cells were seeded in 12- or 6-well plates at 0.8×10^5 cells per well or 1.5×10^5 cells per well for downstream transfections or treatments as needed. HUVECs were experimentally treated or transfected at passages 3 to 5, since after seven passages, cells are more susceptible to senescence. ADSCs were also used at a similar passage number range.

4.5. In Vitro miRNA Transfections and Growth Hormone (GH) Administration. To increase miR-449a expression in vitro, miR-449a-5p miRIDIAN microRNA Mimic (Dharmacon™) was diluted to a concentration of 20 nM per well in serum-free media, combined with Qiagen's HiPerFect transfection reagent, and incubated for 10 min for enhanced transfection efficiency. Cells were then incubated with the prepared transfection mixture for 3 h at 37 °C in a 5% CO_2 incubator prior to adding sufficient supplemented media for continued growth. To inhibit miR-449a expression in vitro, miR-449a 50 nmol miRIDIAN hairpin inhibitor (Dharmacon™) was diluted to a concentration of 25 nM per well in serum-free media and HiPerFect transfection reagent as described above. Transfections were maintained for a total of 72 h prior to change of media or whole-cell lysate collection using Invitrogen™ TRIzol™ Reagent (ThermoFisher Scientific). RNA was isolated through chloroform and ethanol precipitation followed by nucleic acid quantification using the Epoch Gen5 plate reader (BioTek). Inhibitor and mimic dosages were determined based on titrated transfection concentrations conducted in our lab. GH was prepared by diluting somatotropin (Reporcin, Alpharma, Inc.) in RNAse-free water. Ideal GH concentration for in vitro treatments in HUVECs was determined as described in *SI Appendix, Supplemental Methods Section 1.4*.

4.6. In Vitro Cocultures and Exosome Isolation. HUVECs were treated with GH for 5 d and then cocultured with transfected (20 nM) and nontransfected ADSCs for another 5 d with GH supplementation. CELLTREAT Scientific Products (Pepperell) Permeable Cell Culture Inserts (3.0 µm) were used for cocultures. Transfected and nontransfected ADSCs were seeded on permeable inserts following 72 h of transfection time and then transferred to six-well plates containing GH-treated HUVECs. Following treatment, whole-cell lysates were collected from HUVECs, and RNA was isolated followed by RT-qPCR. To isolate exosomes suspended in concentrated conditioned media, media was collected from transfected and nontransfected ADSCs and filtered using Vivaspin centrifugal concentrators optimized for ultrafiltration (Sartorius). Collected exosomes from ADSCs were then subject to lysis and RNA isolation, as described in 4.7., followed by cDNA preparation and RT-qPCR as described in *SI Appendix, Supplemental Methods Section 1.2* (*SI Appendix*, Fig. S10*A*). To evaluate the uptake of exosomes in recipient HUVECs, isolated exosomes were incubated with SYTO™ RNASelect™ Green Fluorescent cell Stain (Invitrogen), washed to remove excess stain, and added to GH-treated HUVECs. Following incubation time (3 h), HUVECs were fixed with 4% paraformaldehyde (ThermoFisher Scientific) and then permeabilized with 0.1% Triton X-100 (Invitrogen). Fixed HUVECs were then blocked with 1% Bovine Serum Albumin (Sigma-Aldrich) and stained with Alexa Fluor™ 594 Phalloidin (Invitrogen). Cells were mounted in ProLong™ Gold Antifade Mountant with DAPI (Life Technologies) prior to imaging and analysis using the All-in-One Keyence Fluorescence Microscope BZ-X800 (Keyence). HUVECs treated with unlabeled exosomes in parallel were subject to WCL lysis, RNA extraction, cDNA prep, and RT-qPCR as described previously.

4.7. Statistical Analysis. All results are presented as mean ± standard error of the mean (SEM). Statistical analysis was conducted using the GraphPad Prism 9.1.0 (221) software via one-way ANOVA with multiple comparisons (Tukey's test) or independent *t* test (if comparing two groups). A P value < 0.05 was considered statistically different. Single-nucleus RNA-sequencing and total vWAT RNA sequencing analyses methods are described in supplemental methods sections 1.5 and 1.6, respectively.

Data, Materials, and Software Availability. All study data are included in the article and/or *SI Appendix*.

ACKNOWLEDGMENTS. This work was supported by NIH grants R15 AG059190 (M.M.M.), R56 AG061414 (M.M.M.), R03 AG059846 (M.M.M.), R21 AG062985 (M.M.M.), R56 AG074499 (M.M.M.), the Florida Legislative Grant 2014-2022 (M.M.M.), Nathan Shock Center, San Antonio, TX (M.M.M.), and European Commission program HORIZON 2020-MSCA-RISE, Marie Sklodowska-Curie Staff Actions (M.M.M. and A.J.). This work also was supported by grants R01DK080157, R01AG075684 (N.M.), RO1AG069690 (N.M.), U54AG075941 (N.M.), P30AG044271 (N.M.), P30AG013319 (N.M.), and T32AG021890 (J.N.) as well as The Richard Tucker Gerontology Applied Research Grant sponsored by the Learning Institute for Elders at the University of Central Florida (S.N.).

Author affiliations: [a]Burnett School of Biomedical Sciences, College of Medicine, University of Central Florida, Orlando, FL 32827; [b]Sam and Ann Barshop Insititute for Longevity and Aging Studies, University of Texas Health Science Center at San Antonio, San Antonio, TX 78229; [c]Faculdade de Nutrição, Universidade Federal de Pelotas, 96010-610 Pelotas, Brazil; [d]Institute on the Biology of Aging and Metabolism, Department of Biochemistry, Molecular Biology and Biophysics, University of Minnesota, Minneapolis, MN 55455; [e]Department of Medical Education, School of Medicine, California University of Science & Medicine, Colton, CA 92324; [f]Celon Pharma Innovative Drugs Research & Development Department, Celon Pharma S.A., 05-152 Kazun Nowy, Poland; [g]San Antonio Geriatric Research Education and Clinical Center (GRECC), South Texas Veterans Health Care System, San Antonio, TX 78229; [h]Department of Medicine, Cedars Sinai Medical Center, LA 90048; and [i]Department of Head and Neck Surgery, Poznan University of Medical Sciences, 60-355 Poznan, Poland

1. A. Bartke *et al.*, Extending the lifespan of long-lived mice. *Nature* **414**, 412 (2001).
2. J. E. Ayala, D. S. Wiesenborn, E. King, M. M. Masternak, Insulin sensitivity in long-living Ames dwarf mice. *Age* **36**, 9709 (2014).
3. M. M. Masternak, J. A. Panici, M. S. Bonkowski, L. F. Hughes, A. Bartke, Insulin sensitivity as a key mediator of growth hormone actions on longevity. *J. Gerontol. Series A Biol. Sci. Med. Sci.* **64A**, 516–521 (2009).
4. V. Menon *et al.*, The contribution of visceral fat to improved insulin signaling in Ames dwarf mice. *Aging cell* **13**, 497–506 (2014).
5. J. Darcy, Y. H. Tseng, ComBATing aging–does increased brown adipose tissue activity confer longevity? *GeroScience* **41**, 285–296 (2019).
6. C. Kang, Senolytics and senostatics: A two-pronged approach to target cellular senescence for delaying aging and age-related diseases. *Mol. Cells* **42**, 821–827 (2019).
7. L. A. MacFarlane, P. A. Murphy, MicroRNA: Biogenesis, function, and role in cancer. *Curr. Genom.* **11**, 537–561 (2010).
8. J. Campisi, Aging, cellular senescence, and cancer. *Annu. Rev. Physiol.* **75**, 685–705 (2012).
9. P. Y. Desprez, J. P. Coppe, A. Krtolica, J. Campisi, The senescence-associated secretory phenotype: The dark side of tumor suppression. *Annu. Rev. Physiol.* **5**, 99–118 (2010).
10. L. N. Yo, B. Victoria, M. M. Masternak, MicroRNAs and the metabolic hallmarks of aging. *Mol. Cell. Endocrinol.* **455**, 131–147 (2017).
11. A. D. C. Nunes *et al.*, miR-146a-5p modulates cellular senescence and apoptosis in visceral adipose tissue of long-lived Ames dwarf mice and in cultured pre-adipocytes. *GeroScience* **44**, 503–518 (2022).
12. Y. A. M. Yusof, S. Khee, S. Makpol, Expression of senescence-associated microRNAs and target genes in cellular aging and modulation by tocotrienol-rich fraction. *Oxid. Med. Cell. Longev.* **2014**, 725929 (2014), 10.1155/2014/725929.
13. B. Victoria *et al.*, Circulating microRNA signature of genotype-by-age interactions in the long-lived Ames dwarf mouse. *Aging cell* **14**, 1055–1066 (2015).
14. J. Darcy, S. McFadden, A. Bartke, Altered structure and function of adipose tissue in long-lived mice with growth hormone-related mutations. *Adipocyte* **6**, 69–75 (2017).
15. M. B. Stout *et al.*, Growth hormone action predicts age-related white adipose tissue dysfunction and senescent cell burden in mice. *Aging* **6**, 575–586 (2014).
16. N. Naderi *et al.*, The regenerative role of adipose-derived stem cells (ADSC) in plastic and reconstructive surgery. *Int. Wound J.* **14**, 112–124 (2017).
17. A. K. Sárvári *et al.*, Plasticity of epididymal adipose tissue in response to diet-induced obesity at single-nucleus resolution. *Cell Metab.* **33**, 437–453 (2021).
18. C. Hepler *et al.*, Identification of functionally distinct fibro-inflammatory and adipogenic stromal subpopulations in visceral adipose tissue of adult mice. *Elife* **7**, e39636 (2018).
19. X. Wang, Y. Chen, miRDB: An online database for prediction of functional microRNA targets. *Nucleic Acids Res.* **48**, D127–D131 (2020), 10.1093/nar/gkz757, D127-D131.
20. S. Vlachos *et al.*, DIANA-miRPath v3.0.: DIANA-miRPath v3.0: Deciphering microRNA function with experimental support. *Nucleic Acids Res.* **43**, W460–W466 (2015).
21. M. Kanehisa, Y. Sato, M. Kawashima, M. Furumichi, M. Tnabe, KEGG as a reference resource for gene and protein annotation. *Nucleic Acids Res.* **44**, D457–D462 (2016).
22. R. A. Avelar *et al.*, A multidimensional systems biology analysis of cellular senescence in aging and disease. *Genome Biol.* **21**, 91 (2020).
23. J. Baker, P. J. Barnes, L. E. Donnelly, Senescence as a mechanism and target in chronic lung diseases. *Am. J. Respir. Crit. Care Med.* **200**, 556–564 (2019).
24. G. J. Lithgow, R. Martins, W. Link, Long live FOXO: Unraveling the role of FOXO proteins in aging and longevity. *Aging cell* **15**, 196–207 (2016).
25. D. Merrick, Identification of a mesenchymal progenitor cell hierarchy in adipose tissue. *Science* **364**, eaav2501 (2019).
26. R. B. Burl *et al.*, Deconstructing adipogenesis induced by β3-adrenergic receptor activation with single-cell expression profiling. *Cell Metab.* **28**, 300–309 (2018).
27. P. C. Schwalie *et al.*, A stromal cell population that inhibits adipogenesis in mammalian fat depots. *Nature* **559**, 103–108 (2018).
28. C. M. Hill *et al.*, Long-lived hypopituitary Ames dwarf mice are resistant to the detrimental effects of high-fat diet on metabolic function and energy expenditure. *Aging cell* **15**, 509–521 (2016).
29. J. Darcy, S. McFadden, A. Bartke, Altered structure and function of adipose tissue in long-lived mice with growth hormone-related mutations. *Adipocyte* **6**, 69–75 (2017).
30. J. H. Park *et al.*, Pharmacological inhibition of mTOR attenuates replicative cell senescence and improves cellular function via regulating the STAT3-PIM1 axis in human cardiac progenitor cells. *Exp. Mol. Med.* **52**, 615–628 (2020).
31. D. E. Harrison *et al.*, Rapamycin fed late in life extends lifespan in genetically heterogeneous mice. *Nature* **460**, 392–395 (2009).
32. D. Lamming, Diminished mTOR signaling: a common mode of action for endocrine longevity factors. *Springer Plus* **3**, 735 (2014).
33. A.-R. Khalid, A. Gesing, A. Bartke, M. M. Masternak, Growth hormone abolishes beneficial effects of calorie restriction in long-lived Ames dwarf mice. *Exp. Gerontol.* **58**, 219–229 (2014).
34. A. El-Badawy *et al.*, Adipose stem cells display higher regenerative capacities and more adaptable electro-kinetic properties compared to bone marrow-derived mesenchymal stromal cells. *Sci. Rep.* **6**, 37801 (2016).
35. S. Paik *et al.*, miR-449a regulates the chondrogenesis of human mesenchymal stem cells through direct targeting of lymphoid enhancer-binding factor-1. *Stem Cells Dev.* **21**, 3298–3308 (2012).
36. E. J. Noonan, R. F. Place, S. Basak, D. Pookot, L. C. Li, miR-449a causes Rb-dependent cell cycle arrest and senescence in prostate cancer cells. *Oncotarget* **1**, 349–358 (2010).
37. Y. X. Tan *et al.*, MicroRNA-449a regulates the progression of brain aging by targeting SCN2B in SAMP8 mice. *Int. J. Mol. Med.* **45**, 1091–1102 (2020).
38. J. Tan, Y. Xu, F. Han, X. Ye, Genetical modification on adipose-derived stem cells facilitates facial nerve regeneration. *Aging* **11**, 908–920 (2019).
39. K. N. Kunze, R. A. Burnett, J. Wright-Chisem, R. M. Frank, J. Chahla, Adipose-derived mesenchymal stem cell treatments and available formulations. *Curr. Rev. Musculoskeletal Med.* **13**, 264–280 (2020).
40. T. Ma *et al.*, A brief review: Adipose-derived stem cells and their therapeutic potential in cardiovascular diseases. *Stem. Cell Res. Therapy* **8**, 124 (2017).